 https://doi.org/10.3311/PPme.20880

Periodica Polytechnica Mechanical Engineering, 68(2), pp. 114–119, 2024

Numerical Investigation on Influence of Grooves on Tube Hydroforming Process of Aluminium Alloys

Ganesh Laxman Ramanathan[1], Ajith Ramesh[1*], Arun Achuthankutty[1]

[1] Department of Mechanical Engineering, Amrita School of Engineering, Coimbatore, Amrita Vishwa Vidyapeetham, India
[*] Corresponding author, e-mail: r_ajith@cb.amrita.edu

Received: 26 July 2023, Accepted: 13 February 2024, Published online: 19 April 2024

Abstract

For several decades, scientists and engineers have been using the tube hydroforming (THF) process for numerous applications in the automotive and aerospace industries. The inert advantages like weight reduction without compromising on strength, improved part quality, better surface finish, and reduced tooling costs have motivated the use of THF in the fabrication industry. The presence of grooves on the pre-forms was found to immensely help in increasing the pressure-withstanding capacity of the THF tubes, in addition to reducing the stress concentration and achieving the near-net shape during the THF process. This project involves the development of a detailed Finite Element Model, for the THF process. Numerical analysis is carried out in two stages: Stage-1: Groove Formation, and Stage-2: Final THF tube formation. In Stage 1, the numerical model investigates the formation of grooves, predicting the amount of internal pressure and axial feeding that are required to accurately form them. In Stage 2, numerical simulations focus on the actual THF process. This two-stage THF process (Grooved-THF) was compared to a single-stage Generic THF process. The results indicate the Grooved-THF to be producing a relatively lower thickness reduction with a more closely formed corner radius compared to the generic case. The work also involves multi-objective optimization of the process parameters like the number of grooves, coefficient of friction, internal fluid pressure, and die corner radius using the DOE technique – RSM. The results indicate the number of grooves and the friction coefficient to be the most influencing parameters in the THF process.

Keywords

generic-THF, Grooved-THF, axial feed, response surface methodology

1 Introduction

Among other conventional fabrication processes, hydroforming is close to net metal forming. It has three types: shell, sheet, and tube [1]. THF is a forming process that creates flawless products by using pressurized fluid. It is possible to produce parts using less labor. Tube hydroforming benefits include re-entrant features like less thinning, improved mechanical properties, improved surface finish, fewer components required during assembly, and less rework. Tube hydroforming has been widely employed to create parts in a variety of fields due to increased demand for lighter parts, utilizing light materials will substantially reduce weight. Because of its special advantage of having uniform thickness distribution and its formability, THF has found employment in the aerospace and automobile industries like camshafts, crankshafts, and spaceframes [1–6]. THF has some drawbacks, despite a wide range of applications such as leakage of pressurized fluid [7, 8], expensive tooling, and process maintenance. Numerous studies on the tube hydroforming method's process parameters have been carried out to understand and eradicate those drawbacks.

Common defects in tube hydroforming are discussed and analyzed numerically in various literature. Tube hydroforming (THF) has common parameters like internal pressure, external pressure, and friction coefficient.

THF utilizes internal pressure and axial feeding with the application of external pressure to form grooves [9]. Many researchers studied this wrinkling/groove formation and the use of wrinkles to form the desired shape [9–13]. Fig. 1 indicates the schematic diagram of THF including axial feeding with internal and external pressure application via left/right punches.

Cite this article as: Ramanathan, G. L., Ramesh, A., Achuthankutty, A. "Numerical Investigation on Influence of Grooves on Tube Hydroforming Process of Aluminium Alloys", Periodica Polytechnica Mechanical Engineering, 68(2), pp. 114–119, 2024. https://doi.org/10.3311/PPme.20880

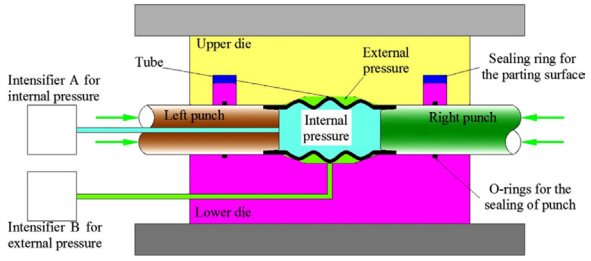

Fig. 1 Schematic diagram of experimental setup [9]

THF has been manufactured using internal and external pressure, a process known as double-sided tube hydroforming [14]. A detailed Finite Element approach has been developed in this work to further research the formation of grooves and the influence of grooves in THF, followed by an extensive optimization methodology to predict optimum parameters and responses using the FEM-based approach as the foundation.

2 Methodology

Numerical analysis using ABAQUS/Explicit package was performed for the formation of grooves (Stage-1), and the grooved tubes were then used to complete the formation of the tube to the required shape (Stage-2). Yuan et al.'s [9, 13] experimental work helped us validate the groove-formed tube model (both Stage-1 and Stage-2). This model is then compared to a single-stage process in which the tube is formed into its final shape (Generic THF).

This comparison will aid in understanding the role of the groove in THF. The Process Diagram for Grooved and Generic THF is shown in Fig. 2. Further to that, for the grooved THF process, a parametric study for Stage 1 and Stage 2 was completed, as well as a multi-objective optimization. Optimization has been carried down using the Response surface methodology (RSM) technique under Central composite design (CCD) by considering critical input parameters. Objectives of optimization are maximizing reduced thickness and minimizing corner radius.

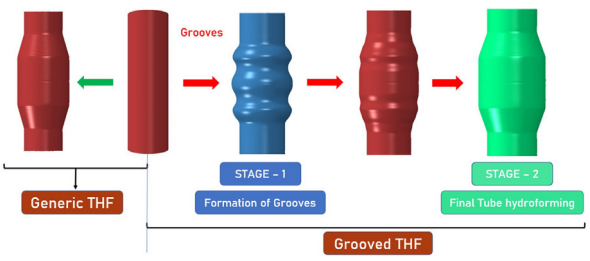

Fig. 2 Process Diagram for Grooved and Generic THF

2.1 Material module

The tube material used in this research is aluminum alloy 5A02. The tube has an outer diameter of 63 mm with a nominal thickness of 2 mm. The material was taken out from the extruded tube and then annealed at 380 ˚C for about 2h [9, 14, 15]. Table 1 shows the mechanical properties of the material.

Holloman Eq. (1) was used to predict the plastic data.

$$\bar{\sigma} = K\bar{\varepsilon}^{n}, \tag{1}$$

where the $\bar{\sigma}$ and $\bar{\varepsilon}$ are equivalent stress and strain, K is the strength coefficient, and n is the strain hardening exponent. The threshold stress at which plastic deformation begins and ends is taken from the literature as 84.1 and 275.4 MPa [9]. These values are fed into Eq. 1 to generate the true stress and strain curve shown in Fig. 3.

The generated true stress and true strain values have been imported to the Abaqus material module for FE Simulations. A total of 320 plastic data values were taken with an interval of 0.5 MPa.

3 Numerical analysis

Finite element modeling is a reliable technique for increasing the understanding of forming processes and predicting the influence of process parameters. The 3D FE modeling and analysis have been developed using ABAQUS/Explicit software.

Table 1 Mechanical parameter of 5A02-O [9, 14, 15]

Mechanical Parameters		Value
Elastic modulus, E (GPa)		70
Yield stress, σ_s (MPa)		85.9
Ultimate tensile strength, σ_b (MPa)		222.9
Total elongation, δ (%)		26.1
Holloman equation	K (MPa)	454.1
	n	0.304

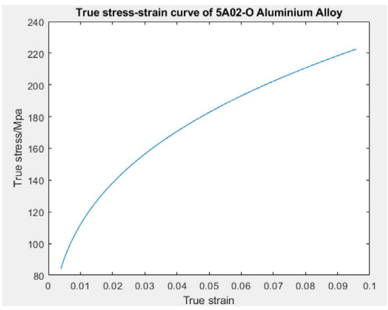

Fig. 3 True stress-strain curve of 5A02 – O aluminum alloy

3.1 Interactions and boundary conditions

The assembly is made up of three major components (shown in Fig 4): 1. Tube Blank 2. Die 3. Punch. Surface-to-surface interactions are defined as those between a tube blank and a die, as well as between a tube blank and a punch. Die and punches are used as masters and tube blanks are used as slaves. The coefficient of friction is 0.125 [9].

In Stage 1 of the grooved THF model, the maximum displacement of 15 mm has been applied to each punch. A uniform pressure load is applied as shown in Fig. 5. The die has been encastered since it doesn't have any movement/displacement.

The loading path used for groove formation is taken from the literature [9]. An additional step with no load acting on the tube is added near the end to reduce spring back and for better stress relaxation [17]. In Stage 2, the grooved tubes were blown up to take the final shape of the die. This model has also been validated using published experimental results [9, 15]. Table 2 and Table 3 compare simulation results to experimental results.

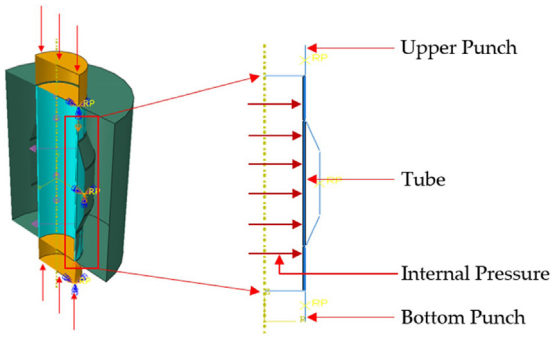

Fig. 4 3D Assembled model with boundary conditions

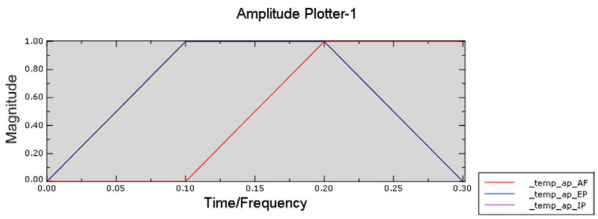

Fig. 5 Loading path – Stage 1

Table 2 Comparison of experimental (from literature) and FEM results of Stage 1 – grooved THF

Groove Height (mm)	Experimental [9]	FE Simulation	Error (%)
Groove 1	40.741	41.493	1.85
Groove 2	42.322	42.393	0.17
Groove 3	40.613	41.506	2.20

The arbitrary Lagrangian-Eulerian (ALE) is used to model the material flow. Lower deformation displacements are solved using a Lagrangian approach in the mesh. Mesh adapts to the Eulerian approach for extensive material flow and solves for velocities [16–21].

In Stage 2, the grooved tube has been used as a blank and expanded to acquire the shape of the die using the loading path shown in Fig. 6.

An eight-node 3D stress linear brick element with reduced integration and hourglass control C3D8R is used for the meshing.

Around 80220 elements were used for discreting the tube blank. We conducted a comprehensive mesh convergence study. The key criterion for determining the optimal mesh size was based on achieving a balance between the accuracy of the numerical results and the computational time required for convergence. Our goal was to identify the mesh size that yielded results in the closest agreement with experimental observations while considering the computational efficiency. The optimization process was performed iteratively, carefully examining various mesh configurations to ensure the robustness and reliability of our simulations.

Time scaling is applied to the model. The simulation took 2.1 seconds to complete. Stage 1 took 0.3 s, followed by Stage 2 taking 1.8 s. Peak pressure for Stage 2 was calculated as 15 times the yield pressure Ps. The tube's initial yield pressure is 5.63 MPa.

Generic THF has the same material module, interactions, and loading path as grooved THF.

Table 3 Comparison of experimental (from literature) and FEM results of Stage 2 – grooved THF

	Experimental [9, 15]	FE Simulation	Error (%)
Total length	180	181.2651	0.34
Average Thickness Reduction	2 mm	1.8172 mm	9.14
Die corner Angle	20°	19.2816°	3.6

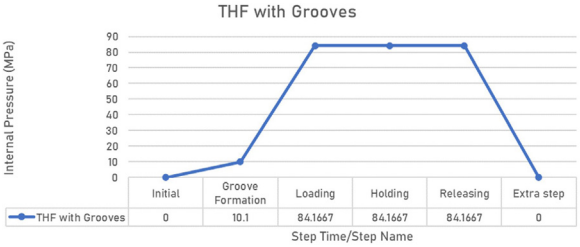

Fig. 6 Loading path – Stage 1 and Stage 2

The FE Model results were validated against the experimental results published in the literature [9, 15]. This work was expanded with a change in the pressure loading path, as shown in Figs. 4, 5. The Grooved THF model is then compared to a generic model, and multi-objective optimization is performed.

4 Results and discussion

The first phase of this research will focus on validating the stage 1 FE model. Groove formation in Stage 1 is depicted in Fig. 7(a). The effect of internal and axial feeding parameters on output parameters such as the number of grooves and groove height is investigated. Table 2 compares the experimental and numerical results in the first stage of groove formation. Stage 1's output was used as the input for Stage 2.

In Stage 2, the grooved tubes were blown up to take the final shape of the die. This model has also been validated using published experimental results [9, 15]. Table 3 compares simulation results to experimental results.

Fig. 7(b) depicts the stress contours at the end of Stage 1. The stress formed at the end of Stage 1 is approximately 221.6 MPa, and the stress formed at the end of Stage 2 is approximately 263.1 MPa. In Stage 2, since the material has previously undergone plastic deformation (Stage 1) to form grooves, dead stresses collect in the grooves of the tube blank during Stage 2, increasing stress by approximately 42 MPa. Fig. 8 depicts the stress contours at the end of Stage 2.

The corner radius and thickness reduction are measured and used as critical output parameters after Stage 2. The corner radius measured for Grooved THF was 8.37117 mm. To investigate the effect of grooves on tube formability, the results of generic and grooved THF are compared. Table 4 contrasts the results of Generic and Grooved THF.

The results show that grooved THF improves average thickness reductions and corner radius significantly. To comprehend the thickness distributions along the length of the tube, a path was constructed and the corresponding thickness at each node was plotted, as shown in Fig. 9.

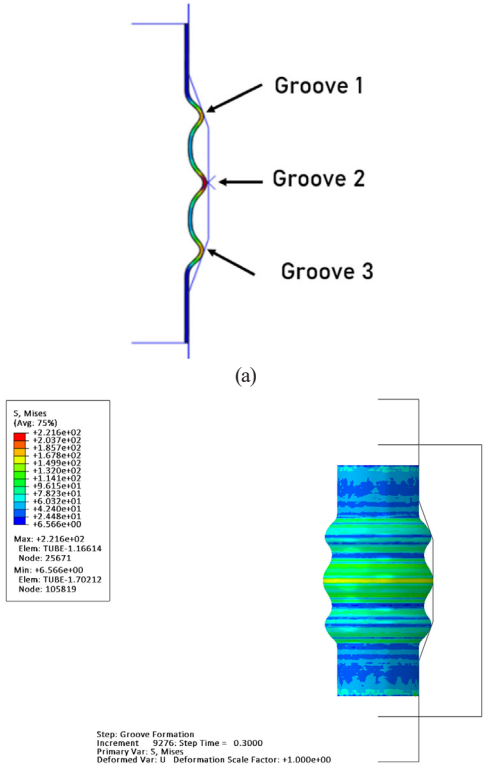

Fig. 7 (a) Stage 1 Groove Formation, (b) Von Mises measurement after Stage 1

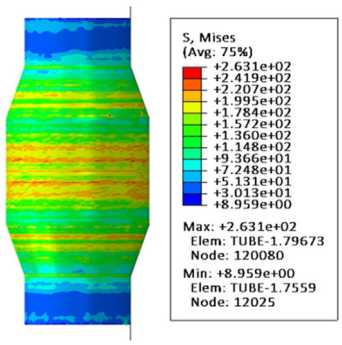

Fig. 8 Von Mises measurement after Stage 2

Table 4 Comparison of grooved THF and generic THF results

	Grooved THF	Generic THF	Improvement (%)
Minimum corner Radius	8.371	13.870	39.64
Average Thickness Reduction	1.817 mm	1.671 mm	8.74
Die corner Angle	19.2816°	16.181°	14.74

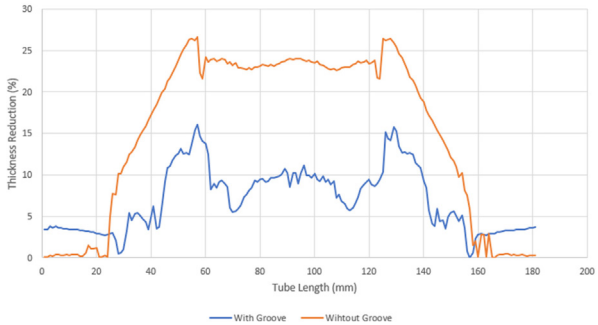

Fig. 9 Percentage thickness reduction – Comparison B/W grooved and generic THF

The highest reduction percentage recorded in generic THF is around 26.65 percent, and the lowest reduction percentage recorded in grooved THF is around 16.06 percent. Variations along the length of the grooved formed tube indicate that more material is accumulated in the tube blank even after Stage 2 deformation. This indicates that the tube can be further formed. Significant variation in thickness along the length direction does not indicate the required output. As a result, the thickness variation along each cross-section was recorded for further analysis. Fig. 10 depicts the thickness of random points selected in each cross-section.

According to the plotted results in Fig. 10, the thickness across each cross section (each point) has a similar reduced thickness. The maximum thickness variation across a cross-section is approximately 0.07844 mm. The change in loading path resulted in less stress concentration and more relaxation and spring-back. As a result, the new loading path and grooved THF produce better results.

The work is further advanced by varying parameters such as friction coefficient, number of grooves, die corner radius, and internal pressure. Response surface methodology (RSM) is used to optimize responses, and an ANOVA table is generated. Table 5 depicts the input parameters and parameter range. Because the interval is not equal, the number of grooves is used as a categorical factor. The zero groove corresponds to generic THF. Figs. 11, 12 show the mean effective plot for minimum corner radius and maximum reduced thickness.

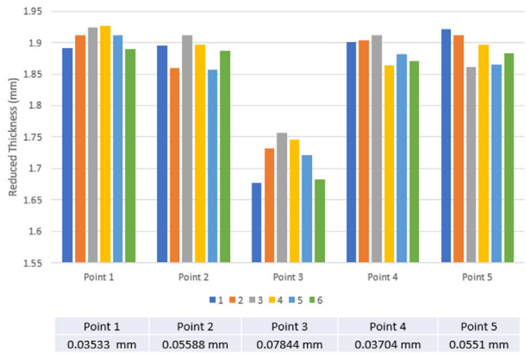

Fig. 10 Reduced Thickness at various cross-sections

Table 5 Optimization parameters and range

	Level 1	Level 2	Level 3
Friction Coefficient	0.04	0.08	0.12
Internal Pressure	80	85	90
Die corner radius	4	6	8
No. of groves	0	2	3

According to the main effect plot, the number of grooves is important in multiobjective optimization, followed by the friction coefficient. Simulation in the validated model is used to confirm the result. Results are shown in Table 6. Because the desirability is greater than 80%, the results are less prone to error.

5 Conclusion

A detailed finite element model for grooved THF is developed and validated using experimental data. The work is improved further by including different loading paths and optimizing parameters and responses by using grooves as a critical parameter. Grooved THF has been found to have improved forming capacity, corner radius, and thickness. The effect of input parameters such as friction coefficient,

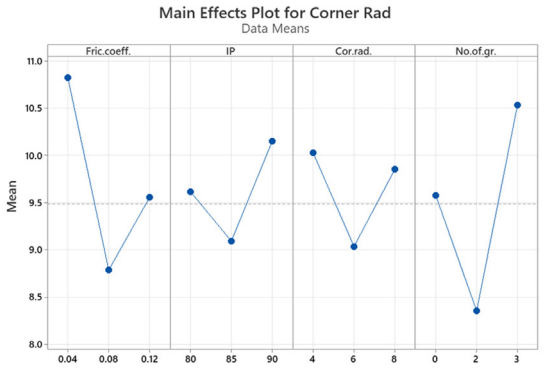

Fig. 11 Main effect plot for minimum corner radius

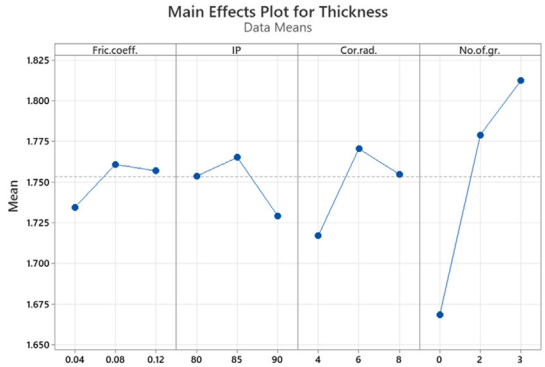

Fig. 12 Main effect plot for maximum reduced thickness

Table 6 Confirmation of results

	Optimized result	Simulation results	Error (%)
Reduced Thickness	1.8367	1.8548	0.816
Corner Radius	7.6323	7.2954	4.414

internal pressure, number of grooves, and die corner radius on output parameters such as minimum corner radius and maximum reduced thickness for the THF is investigated. It has been discovered that grooved THF produces better and more optimal results than generic THF. The reduced thickness has improved by 8.74 percent, and the corner radius has improved by 39.64 percent. The optimization studies show that the optimum values for the coefficient of friction, internal pressure, corner radius, and the number of grooves are 0.0966, 80 MPa, 6.67 mm, and 2 respectively. Numerical results validate optimized responses.

References

[1] Bell, C., Corney, J. R., Zuelli, N., Savings, D. "A state of the art review of hydroforming technology", International Journal of Material Forming, 13(5), pp. 789–828, 2019. https://doi.org/10.1007/s12289-019-01507-1

[2] Ashwak, A., Bhil, A., Manjunath, V. B. "A Review on Tube Hydroforming (THF) Technology for Automotive Application", International Research Journal of Multidisciplinary Technovation, 1(1), pp. 11–18, 2019. https://doi.org/10.34256/irjmt1912

[3] Parekh, V. R., Shah, J., Patel, B. C. "Review on Tube Hydroforming Process with Considerable Parametric Effect", International Journal on Theoretical and Applied Research in Mechanical Engineering, 1(1), pp. 117–123, 2012.

[4] Koç, M., Altan, T. "An overall review of the tube hydroforming (THF) technology", Journal of Materials Processing Technology, 108(3), pp. 384–393, 2001. https://doi.org/10.1016/S0924-0136(00)00830-X

[5] Lang, L. H., Wang, Z. R., Kang, D. C. Yuan, S. J., Zhang, S. H., Danckert, J., Nielsen, K. B. "Hydroforming highlights: sheet hydroforming and tube hydroforming", Journal of Materials Processing Technology, 151(1–3), pp. 165–177, 2004. https://doi.org/10.1016/j.jmatprotec.2004.04.032

[6] Alaswad, A., Benyounis, K. Y., Olabi, A. G. "Tube hydroforming process: A reference guide", Materials & Design, 33, pp. 328–339, 2012. https://doi.org/10.1016/j.matdes.2011.07.052

[7] Park, J. Y., Sang, W. H., Jeong, H. S., Cho, J.-R., Moon, Y. M. "Advanced sealing system to prevent leakage in hydroforming", Journal of Materials Processing Technology, 247, pp. 103–110, 2017. https://doi.org/10.1016/j.jmatprotec.2017.04.006

[8] Jeong, H. S., Han, S. W., Ra, J. H., Moon, Y. H. "Application of segmented rubber rings to increase the sealing efficiency in hydroforming", Journal of Mechanical Science and Technology, 32(7), pp. 3153–3159, 2018. https://doi.org/10.1007/s12206-018-0618-6

[9] Yuan, S. J., Cui, X. L., Wang, X. S. "Investigation into wrinkling behavior of thin-walled 5A02 aluminum alloy tubes under internal and external pressure", International Journal of Mechanical Sciences, 92, pp. 245–258, 2015. https://doi.org/10.1016/j.ijmecsci.2014.12.017

[10] Song, W.-J., Kim, S.-W., Kim, J., Kang, B.-S. "Analytical and numerical analysis of bursting failure prediction in tube hydroforming", Journal of Materials Processing Technology, 164–165, pp. 1618–1623, 2005. https://doi.org/10.1016/j.jmatprotec.2005.01.008

[11] Lang, L., Li, H., Yuan, S., Danckert, J., Nielsen, K. B. "Investigation into the pre-forming's effect during multi-stages of tube hydroforming of aluminum alloy tube by using useful wrinkles", Journal of Materials Processing Technology, 209(5), pp. 2553–2563, 2009. https://doi.org/10.1016/j.jmatprotec.2008.06.027

[12] Cui, X. L., Wang, X. S., Yuan, S. J. "Wrinkling behavior in tube hydroforming coupled with internal and external pressure", In: 4th International Conference on New Forming Technology (ICNFT 2015), Glasgow, UK, 2015, pp. 371–377. ISBN: 9781510809772 https://doi.org/10.1051/matecconf/20152106002

[13] Yuan, S., Yuan, W., Wang, X. "Effect of wrinkling behavior on formability and thickness distribution in tube hydroforming", Journal of Materials Processing Technology, 177(1–3), pp. 668–671, 2006. https://doi.org/10.1016/j.jmatprotec.2006.04.101

[14] Cui, X. L., Wang, X. S., Yuan, S. J. "Deformation analysis of double-sided tube hydroforming in square-section die", Journal of Materials Processing Technology, 214(7), pp. 1341–1351, 2014. https://doi.org/10.1016/j.jmatprotec.2014.02.005

[15] Wang, X. S., Cui, X. L., Yuan, S. J. "Research on flattening behavior of wrinkled 5A02 aluminum alloy tubes under internal pressure", International Journal of Advanced Manufacturing Technology, 87, pp. 1159–1167, 2016. https://doi.org/10.1007/s00170-016-8529-0

[16] Shrinaath, V., Vairavignesh, R. , Padmanaban, R. "Parametric Study on the Spring-Back Effect in AA5052 Alloy in the Course of Three-Point Roll Bending Process", Acta Mechanica et Automatica, 14(3), pp. 128–134, 2020. https://doi.org/10.2478/ama-2020-0019

[17] Sumesh, C. S., Ramesh, A. "Numerical Modelling and Optimization of Dry Orthogonal Turning of Al6061 T6 Alloy", Periodica Polytechnica Mechanical Engineering, 62(3), pp. 196–202, 2018. https://doi.org/10.3311/PPme.11347

[18] Surendran, S. B. T., Sumesh, C. S., Ramesh, A. "Numerical Modeling and Optimization of Cold Rolling Process of AA5086 Sheets", Academic Journal of Manufacturing Engineering, 18(3), pp. 168–175, 2020. https://doi.org/10.1007/978-981-15-4745-4_44

[19] Sumesh, C. S., Ramesh, A. "Numerical Modelling and Optimization of Dry Orthogonal Turning of Al6061 T6 Alloy", Periodica Polytechnica Mechanical Engineering, 62(3), pp. 196–202, 2018. https://doi.org/10.3311/PPme.11347

[20] Raut, S. V., Ramesh, A., Arun, A., Sumesh, C. S. "Finite element analysis and optimization of tube hydroforming process", Materials Today: Proceedings, 46, pp. 5008–5016, 2021. https://doi.org/10.1016/j.matpr.2020.10.394

[21] Krishnakumar, P., Prakash Marimuthu, K., Rameshkumar, K., Ramachandran, K. I. "Finite element simulation of effect of residual stresses during orthogonal machining using ALE approach", International Journal of Machining and Machinability of Materials, 14(3), pp. 213–229, 2013. https://doi.org/10.1504/IJMMM.2013.056363